Design and Analysis of an Underactuated Three-Section Link Finger Mechanism

ME5250 Fall 2025 - Project 1 | Report by Ahmad Hassan

1. Introduction

This project explores an underactuated robotic finger mechanism (Option 4), developing a single-actuator system capable of adaptive grasping through geometric constraints. The human hand's 29 degrees of freedom (5 in thumb, 6 per finger) makes full actuation impractical due to cost and complexity. By leveraging mechanical intelligence through linkage design, this underactuated mechanism reduces a 6-DOF finger to single-actuator control while maintaining functional grasping capabilities.

2. Literature Review

2.1 Biomechanical Foundations

Research on hand exoskeleton design revealed finger joint ranges critical for grasping: MCP (0-90°), PIP (0-110°), and DIP (0-70°). This established that exact biomimicry is unnecessary; functional grasping requires only appropriate workspace coverage rather than full 6-DOF replication.

2.2 Underactuated Mechanism Approaches

Five primary strategies exist: tendon-driven (In & Cho, 2015), spring-based (Catalano et al., 2014), compliant mechanisms (Dollar & Howe, 2010; Deimel & Brock, 2016), geometry-based linkages (Birglen & Gosselin, 2004), and hybrid approaches (Aukes et al., 2014). The geometry-based approach was selected for deterministic behavior, mechanical robustness, and 3D printing compatibility, achieving predictable adaptive grasping without maintenance-prone cables or limited-force soft materials.

2.3 Three-Section Link Design

The three-section link mechanism uses cascading four-bar linkages to create natural finger curling motion through mechanical intelligence alone, eliminating sensor requirements while maintaining adaptive capabilities.

3. Mechanism Design and Analysis

3.1 Design Methodology

The mechanism was reverse-engineered from existing three-section link finger implementations through video analysis. The final design consists of nine links (including ground) interconnected through 10 revolute joints and 1 prismatic joint, driven by a single linear actuator. The mechanism achieves coordinated flexion of three phalanx segments through coupled four-bar linkages. The reverse-engineering process involved frame-by-frame analysis to identify joint locations and motion sequences, followed by iterative refinement through kinematic simulation. The CAD model developed in SolidWorks underwent multiple iterations to optimize link proportions and eliminate discontinuous motion.

3.2 Mobility Analysis

The degree of freedom analysis was performed using Grubler's equation for planar mechanisms where m = 3 (planar motion), N = 9 (number of links including ground), J = 11 (number of joints: 10 revolute + 1 prismatic) and Σf = 11 (sum of joint freedoms).

$$DOF = 3(9 - 1 - 11) + 11 = -9 + 11 = 2$$

This analysis confirms the mechanism possesses 2 degrees of freedom while being controlled by a single linear actuator, demonstrating its underactuated nature. Additional degree of freedom enables adaptive behavior when contacting objects of varying geometries.

3.3 Forward Kinematics

The forward kinematic analysis initially appeared intractable due to the mechanism's multiple interconnected closed loops. Traditional serial-chain methods using DH parameters were inapplicable, and attempting to solve all loops simultaneously would yield high-order polynomials. The breakthrough came from recognizing that the closed loops could be analyzed separately by decomposing the mechanism into distinct kinematic subsystems, each solvable analytically. The system transitions between two distinct configurations at a critical angle, requiring separate kinematic models for each phase.

Slider-Crank Analysis: The base actuation was isolated as an independent slider-crank mechanism. The relationship between actuator displacement (d) and crank angle (θ) was derived using the law of cosines: $cos(\theta) = (r^2 + d^2 - l^2)/(2rd)$, providing exact solutions without iteration.

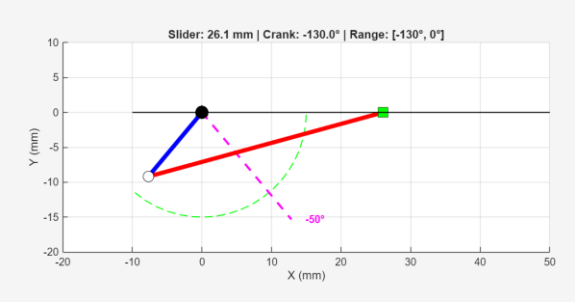

Figure 1: Slider-crank base actuation showing crank angle θ=-130° to 0° with switching point at θ=-50°.

Phase 1: Rigid Body Kinematics ($\boldsymbol{\theta} \in [-\mathbf{130}°, -\mathbf{50}°]$): Analysis revealed that in this range, despite having multiple loops, the four-bar linkage behaves as a rigid assembly. This insight simplified the forward kinematics to rotation matrix transformations, with linear mapping from crank angle to assembly rotation.

Phase 2: V-Linkage Kinematics ($\theta \in [-50°, 0°]$): At θ=-50°, the mechanism transitions to articulated V-linkages with coupled loops. Rather than solving simultaneous constraint equations, each link constraint was reformulated as a geometric circle. The intersection points are computed analytically using the quadratic formula, yielding two possible configurations. Selection based on configuration continuity ensures smooth motion.

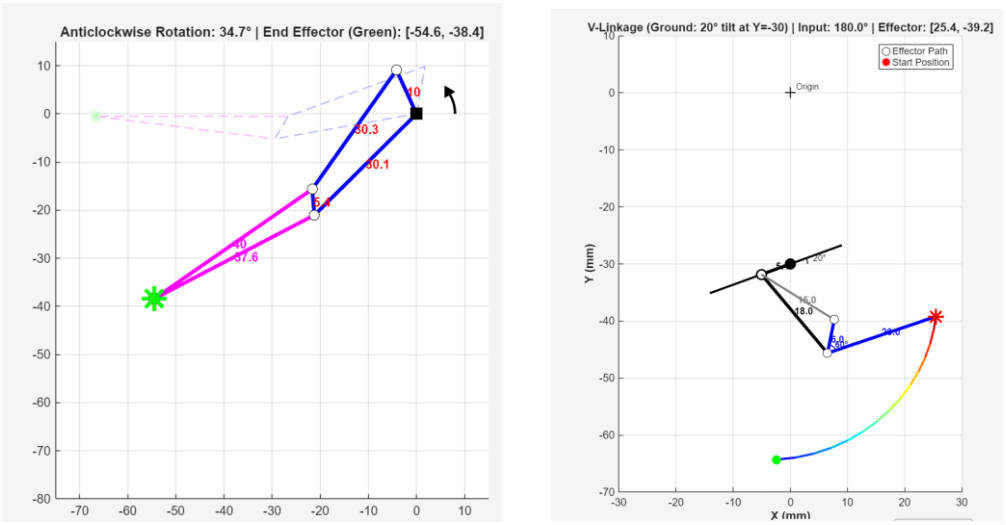

Figure 2a: Rigid link configuration. Figure 2b: V-linkage configuration demonstrating articulated motion with end effector trajectory

Implementation and Validation: The decomposition strategy enabled complete analytical solutions implemented in MATLAB. Initial simulations revealed solution branch discontinuities causing jerky motion. Systematic analysis of both solution branches at each configuration identified optimal selection criteria. The final implementation provides real-time computation with smooth phase transitions, validating that complex closed-loop

mechanisms can be solved analytically through proper decomposition rather than numerical methods.

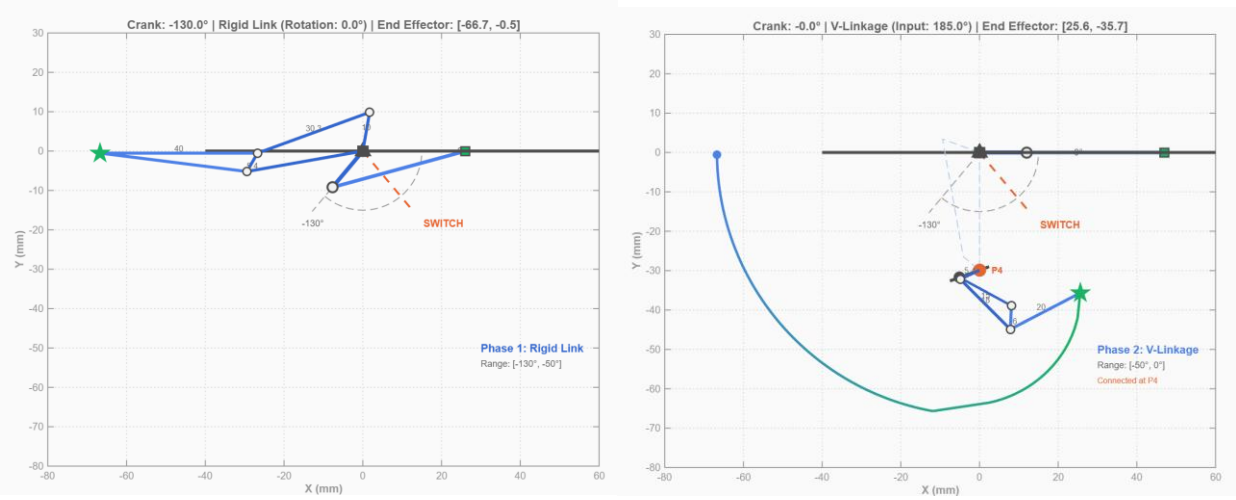

Figure 3: Combined mechanism workspace showing Phase 1 (rigid link, blue) and Phase 2 (V-linkage, green)

4. Results and Discussion

4.1 Range of Motion

The mechanism operates through a linear actuator stroke of 26.1-47mm, driving the crank through $\theta \in [-130°, 0°]$. Phase 1 (Rigid Link, $\theta \in [-130°, -50°]$) rotates the assembly from 0° to ~80°, while Phase 2 (V-Linkage, $\theta \in [-50°, 0°]$) provides articulated motion with input angles 130°-185°. The end-effector traverses from [-66.7,-0.5]mm to [25.6,-35.7]mm, creating a sweeping arc workspace of approximately 92mm×65mm. The smooth transition at θ=-50° validates the kinematic continuity between phases.

4.2 Singularities

Analysis of the kinematic constraints reveals potential singularities when $\cos(\theta)$ approaches ±1 in the slider-crank equation, corresponding to full extension or folding. However, the mechanism operates within $\theta \in [-130°, 0°]$, avoiding these conditions. The V-linkage could encounter singularities if constraint circles fail to intersect, but the design parameters ensure valid intersections throughout the workspace. No operational singularities occur within the design range.

Minor discontinuities in the MATLAB visualization stem from the implementation complexity of coordinating the rigid body and V-linkage reference frames—an implementation challenge rather than a mechanical limitation.

Video Documentation

SOLIDWORKS & MATLAB demonstration available at: https://drive.google.com/file/d/1M96xGyKvcZoVZR8mid9pmtTU457SAQWX/view?usp=sharing

Motion Study Analysis: https://drive.google.com/file/d/1-68JrNohpKwDOeUQaye0mxrodCDTMVU5/view?usp=sharing

3D Printed Model Range of Motion: https://drive.google.com/file/d/11Z55oL1y_YE5IJULBpSN34mm9pxXb91t/view?usp=sharing

Code Repository

MATLAB implementation: https://github.com/ahmadhassan-2609/ME5250-Project-1-Underactuated-Finger-Mechanism.git

References

1. Aukes, D.M., Heyneman, B., Ulmen, J., Stuart, H., Cutkosky, M.R., Kim, S., Garcia, P., & Edsinger, A. (2014). Design and testing of a selectively compliant underactuated hand. *Int. J. Robot. Res.*, 33(5), 721-735.
2. Birglen, L., & Gosselin, C.M. (2004). Kinetostatic analysis of underactuated fingers. *IEEE Trans. Robot. Autom.*, 20(2), 211-221.
3. Catalano, M.G., Grioli, G., Farnioli, E., Serio, A., Piazza, C., & Bicchi, A. (2014). Adaptive synergies for the design and control of the Pisa/IIT SoftHand. *Int. J. Robot. Res.*, 33(5), 768-782.
4. Deimel, R., & Brock, O. (2016). A novel type of compliant and underactuated robotic hand for dexterous grasping. *Int. J. Robot. Res.*, 35(1-3), 161-185.
5. Dollar, A.M., & Howe, R.D. (2010). The highly adaptive SDM hand: Design and performance evaluation. *Int. J. Robot. Res.*, 29(5), 585-597.
6. In, H., & Cho, K.J. (2015). Analysis of the forces on the finger joints by a joint-less tendon-driven finger exoskeleton. *IEEE ICORR*, 235-240.
7. Xia, K., Chen, X., Chang, X., Liu, C., Guo, L., Xu, X., Lv, F., Wang, Y., Sun, H., & Zhou, J. (2022). Hand exoskeleton design and human-machine interaction strategies for rehabilitation. *Bioengineering*, 9(11), 682.